Single-cycle strong terahertz pulse generation from a vacuum-plasma interface driven by intense laser pulses

X. G. Dong,[1] Z. M. Sheng,[1,2,*] H. C. Wu,[3] W. M. Wang,[1] and J. Zhang[1,2]

[1]*Beijing National Laboratory of Condensed Matter Physics, Institute of Physics, CAS, Beijing 100190, China*
[2]*Department of Physics, Shanghai Jiao Tong University, Shanghai 200240, China*
[3]*Max-Planck-Institut für Quantenoptik, D-85748 Garching, Germany*

Single-cycle strong terahertz pulses can be generated by irradiating ultrashort intense laser pulses onto a tenuous plasma slab. At the plasma surface, laser ponderomotive force accelerates electrons and induces net currents, which radiate terahertz pulses. Our theoretical model suggests that if $\tau_L > 2\pi/\omega_p$, with τ_L as the laser-pulse duration and ω_p as the plasma frequency, the emission frequency is around τ_L^{-1}. On the other hand, the emission frequency is around $\omega_p/2\pi$ if $\tau_L < 2\pi/\omega_p$. Our numerical simulations support the theoretical model, showing that such a terahertz source is capable of providing megawatt power, field strengths of MV/cm, and broad frequency tunability.

　　　　PACS number(s): 52.25.Os, 42.65.Re, 52.59.Ye, 52.65.Rr

I. INTRODUCTION

Recently, strong terahertz electromagnetic pulse generation has been attracting great interest, since terahertz radiation potentially has wide applications in terahertz imaging, material characterization, and tomography [1,2]. Typical laser-based terahertz emitters are electro-optic crystals, semiconductors, photoconductive antennas, etc. However, due to the breakdown limit and low conversion efficiencies, it is difficult to obtain powerful terahertz sources with these schemes. Instead, terahertz radiation produced from electron-beam-based and laser-plasma-based emitters were proposed, such as transition radiation of electron beams [3], synchrotron radiation from accelerator electrons [4], Cherenkov wake radiation in magnetized plasmas [5], coherent radiation from plasma oscillations driven by ultrashort laser pulses [6], and radiation from plasma channels and formed filaments of an intense laser pulse propagating in air [7–10]. Some of these schemes can produce high-peak and/or high-average-power terahertz emission, though their conversion efficiencies remain low.

In 2005 we suggested a scheme for high-efficiency terahertz emission based on the excitation of laser wakefield in inhomogeneous plasmas through linear mode conversion [11]. Later Wu *et al.* [12] proposed another terahertz-emission scheme based on the laser wakefield excitation in a thin plasma slab with the thickness around a terahertz wavelength, in which a single-cycle terahertz pulse at the corresponding plasma frequency is radiated from a transient net current driven by the laser ponderomotive force. Compared with the other schemes mentioned above, both schemes can lead to table-top terahertz sources with the electric field strength over 1 MV/cm and the power beyond 1 MW. These powerful terahertz rays could be used for the study of high-field terahertz science [13].

In this paper, we extend our previous work on single-cycle terahertz emissions [12] and consider a longer driving

*zmsheng@aphy.iphy.ac.cn

laser pulse with the duration $\tau_L > 2\pi/\omega_p$, where $\omega_p = \sqrt{ne^2/m\varepsilon_0}$ is the plasma frequency, and n is electron density. We find that the emission frequency is simply about τ_L^{-1}, and the plasma slab need not be close to plasma wavelength λ_p, provided the inhomogeneity region near the vacuum-plasma interface is less than λ_p, where $\lambda_p = 2\pi c/\omega_p$. The advantage with a thin plasma slab with the thickness of $\sim\lambda_p$ is that both the forward and backward emitted terahertz pulses are in single cycle and of comparable magnitudes regardless of the density profile.

The paper is organized as follows. In Sec. II, based on one-dimensional (1D) particle-in-cell (PIC) simulation, a theoretical model is developed for terahertz pulse generation by the action of laser ponderomotive force on a plasma slab. The scaling predicted by the theoretical model is confirmed by further numerical simulations. The effects of plasma inhomogeneity at the plasma boundary are discussed. To illustrate multidimensional properties of terahertz emissions, two-dimensional (2D) PIC simulation results are presented in Sec. III. Finally, a conclusion is given in Sec. IV.

II. 1D PARTICLE-IN-CELL SIMULATIONS AND MODEL CALCULATION

A. 1D PIC simulation results

Let us consider that a plane femtosecond laser pulse is obliquely incident onto a tenuous plasma slab at an angle of α, as shown in Fig. 1. The plasma slab is underdense and has a sharp surface and a width of several λ_p along the x direction. For simplification, the incident laser pulse is assumed to have a sine longitudinal profile $a_L = a_0 \sin[\pi(t-x/c)/\tau_L]\sin(kx-\omega t)$ for $0 \le (t-x/c) \le \tau_L$ and $a_L = 0$ otherwise. It hits the left boundary of the plasma with s polarization in order to distinguish it easily from the p-polarized terahertz emission. Here $a_L = eA_L/mc$ is the normalized laser vector potential with the peak amplitude a_0, which is related to the light intensity through $I = a_0^2 \times 1.37 \times 10^{18}$ $(\mu m/\lambda)^2$ W/cm^2, where λ is the laser wavelength in vacuum. We take initial plasma density $n = 0.01 n_c$, which
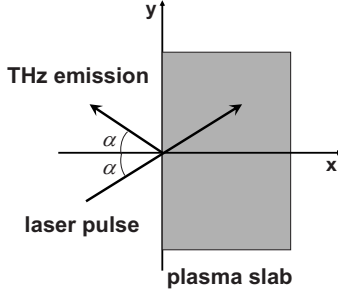
FIG. 1. Schematic of single-cycle terahertz emission from the vacuum-plasma interface generated by a laser pulse obliquely incident onto a plasma slab.

corresponds to $\lambda_p = 10\lambda$. Here, $n_c = m\varepsilon_0\omega^2/e^2 = 1.1 \times 10^{21} \ (\mu m/\lambda)^2$ cm^{-3} is the critical density for a laser pulse with wavelength λ. The plasma slab is localized from $x = 200\lambda$ to $x = 300\lambda$ in a 400λ-long simulation box. In addition we retain a free parameter λ in the presentation of simulation results, so that one can scale to any laser wavelength. For $\lambda = 1 \ \mu m$, one has $n_c = 1.1 \times 10^{21}$ cm^{-3} and $n = 1.1 \times 10^{19}$ cm^{-3}.

Our 1D PIC code adopts a boosted frame moving along y direction in order to deal with the oblique incidence of the laser pulse [14]. Defining fields $F_\pm = (E_y \pm cB_z)/2$ in the moving frame, we see that F_+ and F_- represent the forward and backward p-polarized electromagnetic waves, respectively. Here we mainly focus on analyzing F_- emitted from the left boundary of the plasma slab and obtain the temporal profile of the radiated terahertz pulses in the reflection direction.

Figure 2(a) illustrates the temporal profiles of the terahertz pulses with different laser durations $\tau_L = 20\tau_0$, $40\tau_0$, and $60\tau_0$, where $\tau_0 = \lambda/c$ is the laser oscillation period. The laser amplitude is $a_0 = 0.2$ ($I = 5.5 \times 10^{16}$ W/cm^2 for $\lambda = 1 \ \mu m$),
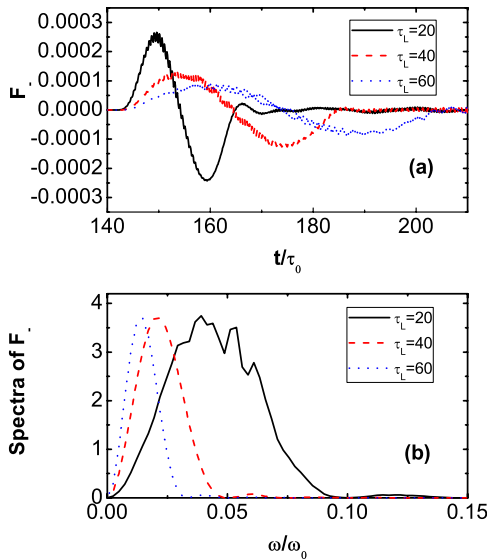

FIG. 2. (Color online) (a) Temporal profiles and (b) frequency spectra (arbitrary units) of the terahertz waves F_-. We take $n/n_c = 0.01$ and laser pulses with $a_0 = 0.2$ and $\alpha = 45°$, and different durations $\tau_L = 20\tau_0$, $40\tau_0$, and $60\tau_0$.

and the incidence angle is $\alpha = 45°$. One find that the radiated terahertz pulse is single cycle, and its duration is almost equal to the incident laser duration. As the duration increases, the terahertz pulse becomes weaker. In all these three cases, we observe that the radiation amplitude $F_- \approx 10^{-4}$ in vacuum, which exceeds 1 MV/cm for the electric field. Spectra of F_- in Fig. 2(b) show that the central frequency of the pulses is around $2\pi/\tau_L$, which is around several terahertz for $\lambda = 1 \ \mu m$. In addition, Fig. 2(a) shows that there are 2ω oscillations riding on the terahertz wave, which is most obvious for the case with $\tau_L = 60\tau_0$. These features are closely related to the laser ponderomotive force, which is in the form $F_p = -mc^2 \nabla a_L^2/2$ in the weakly relativistic limit ($a_L^2 \ll 1$) [15]. For a linearly polarized light, $a_L^2 = a_p^2[1 - \cos(2kx - 2\omega t)]/2$, with as a_p the pulse profile, it shows that F_p contains two time scales: pulse durations τ_L associated with a_p and 2ω oscillations, which corresponds to terahertz and 2ω components in radiation fields as shown in Fig. 2(a).

In our previous study [12], if the laser duration τ_L is around or shorter than $2\pi/\omega_p$, high-amplitude laser wakefields can be generated, and emitted terahertz waves have central frequencies of around ω_p. The presented results in Fig. 2 represent a different regime.

B. Theoretical model

To explain simulation results above, we derive a model for the terahertz radiation from laser-induced plasma transverse currents at plasma surface. As shown later, it is different from terahertz generation by transient longitudinal currents due to photo-Dember or surface field mechanisms in semiconductors [16]. Following Ref. [17], one transforms all variables from the laboratory frame to a moving frame with the velocity $c\sin\alpha \mathbf{e}_y$, where $\mathbf{e}_y$ is a unit vector along the y direction. In this frame, plasmas stream along $\mathbf{e}_y$ with a relativistic factor $\gamma_0 = 1/\cos\alpha$. The assumption of translational symmetry in the moving frame implies that possible plasma perturbations in y or z direction are excluded and the description is restricted to light reflection in the specular direction. Maxwell's equations lead to

$$\left(\partial_x^2 - \frac{1}{c^2}\partial_t^2\right)\mathbf{A}(x,t) = -\frac{1}{\varepsilon_0 c^2}\mathbf{j}_\perp(x,t), \tag{1}$$

$$\partial_x^2\varphi(x,t) = -\frac{1}{\varepsilon_0}\rho(x,t). \tag{2}$$

Here, $\mathbf{A}$ and φ are the vector and scale potentials, respectively, $\mathbf{j}_\perp$ is the electron current in y or z direction, and ρ is the charge density.

The particle's velocity $\mathbf{v}$, momentum $\mathbf{p}$, and relativistic factor γ are related by

$$\mathbf{p} = m\gamma\mathbf{v}, \quad \gamma = \sqrt{1 + \left(\frac{\mathbf{p}}{mc}\right)^2}. \tag{3}$$

Because of the conservation of the generalized transverse momentum, one has

$$d_t(\mathbf{p}_\perp + q\mathbf{A}) = \mathbf{0}, \tag{4}$$

which leads to

$$\mathbf{p}_\perp = m\gamma\mathbf{v}_\perp = \mathbf{p}_\perp^0 - q\mathbf{A}, \tag{5}$$

where $\mathbf{p}_\perp^0 = m\gamma^0\mathbf{v}_\perp^0 = -\mathbf{e_y}mc\tan\alpha$ denotes the initial transverse momentum of the plasma streaming in negative y direction. The initial distributions of electrons and ions are given by $n_e = Zn_i(x) = n_0\Theta(x)$, where n_0 is the electron density of the unperturbed plasma in the moving frame, and $\Theta(x)$ is the profile function of the plasma density.

Substituting Eq. (5) into the transverse current $\mathbf{j}_\perp = -e(n_e\mathbf{v}_{\perp,\mathbf{e}} - Zn_i\mathbf{v}_{\perp,\mathbf{i}})$ in Eq. (1), one can derive a set of equations regarding the vector and scalar potentials for the wakefield and its emission, which are the same as those given by Lichters *et al.* [17] derived for high-harmonic generation from a solid surface. These equations are listed as follows:

$$\left(\partial_x^2 - \frac{1}{c^2}\partial_t^2\right)\mathbf{a_T} = \left(\frac{\omega_p}{c}\right)^2 \mathbf{s}(x,t), \tag{6}$$

$$\partial_x^2\varphi = \left(\frac{\omega_p}{c}\right)^2 \frac{1}{\cos\alpha}[n - \Theta(x)], \tag{7}$$

$$\gamma = \sqrt{\frac{1 + (\mathbf{a_L} - \mathbf{e_y}\tan\alpha)^2}{1 - \beta_x^2}}, \tag{8}$$

$$\mathbf{s}(x,t) = \frac{n}{\gamma\cos\alpha}(\mathbf{a_L} - \mathbf{e_y}\tan\alpha) + \Theta(x)\mathbf{e_y}\tan\alpha, \tag{9}$$

where $\mathbf{a_T}$ and $\mathbf{a_L}$ are the respective vector potentials of the terahertz wave and incident laser normalized by mc/e, φ is the scalar potential of the driven plasma wave normalized by mc^2/e, n is normalized by n_0, and $\mathbf{s}(x,t)$ is the terahertz radiation source. Here we also have assumed that $|\mathbf{a_T}| \ll |\mathbf{a_L}|$, which is generally applicable as found in the numerical simulation.

By adopting the quasistatic approximation [18], we obtain

$$n = \frac{\Theta(x)}{2}\left[\frac{(1 + a_L^2\cos^2\alpha)}{(1 + \varphi\cos\alpha)^2} + 1\right], \tag{10}$$

$$\partial_x^2\varphi = \left(\frac{\omega_p}{c}\right)^2 \frac{\Theta(x)}{2\cos\alpha}\left[\frac{(1 + a_L^2\cos^2\alpha)}{(1 + \varphi\cos\alpha)^2} - 1\right]. \tag{11}$$

In the weak relativistic case $|\varphi| \ll 1$ and $(a_0\cos\alpha)^2 \ll 1$, Eq. (11) can be reduced to

$$\partial_x^2\varphi + k_p^2\Theta(x)\varphi = \frac{k_p^2}{2}\Theta(x)a_L^2\cos\alpha, \tag{12}$$

where $k_p = \omega_p/c = 2\pi/\lambda_p$. For a homogeneous plasma slab $\Theta(x) = 1$, we take $\varphi = 0$ and $\partial\varphi/\partial\xi = 0$ at $\xi = x - ct = 0$ as the boundary conditions, and we find that the scalar potential within the laser pulse is given by

$$\varphi(\xi) = \frac{a_0^2\cos\alpha}{4}\left[1 - \frac{k_p^2\cos(k_l\xi) - k_l^2\cos(k_p\xi)}{k_p^2 - k_l^2}\right], \tag{13}$$

where $k_l = 2\pi\cos\alpha/d_L$ and $d_L = c\tau_L$, and terms of order $(\lambda/\lambda_p)^2 \ll 1$ and $(\lambda/d_L)^2 \ll 1$ have been neglected.

For long laser pulses satisfying the relation $k_l^2 \ll k_p^2$, φ can be approximated by

$$\varphi(\xi) = \frac{a_0^2\cos\alpha}{4}[1 - \cos(k_l\xi)]. \tag{14}$$

In the weakly relativistic case using Eqs. (7), (9), and (14) together, the source equation for s-polarization incidence laser pulse becomes

$$\mathbf{s_y}(x,t) = \frac{a_0^2\sin\alpha\cos\alpha}{4}k_l^2\cos(k_l\xi), \tag{15}$$

which is in the y direction. It indicates that the terahertz emission is always p polarized. The generation of the terahertz radiation is determined by Eq. (6), from which the electric field in the laboratory frame is found to be

$$E_T(x,t) = \frac{\omega_p^2}{2c\omega\cos\alpha}\int_0^{ct} dx'\,\mathbf{s_y}(x',t-|x-x'|/c), \tag{16}$$

where E_T is normalized by $mc\omega/e$. The source $\mathbf{s_y}$ is localized from the surface $x = 0$ to the front of the laser pulse $x = ct$. The integral can be solved as

$$E_T(x,t) = \frac{a_0^2\sin\alpha}{8}\frac{\lambda}{d_L}\{\sin[k_l(x+ct)] - \sin[k_l(x-ct)]\}. \tag{17}$$

This equation shows that the terahertz emission is composed of two parts, which propagate in the specular reflection and laser transmission directions, respectively. Let us consider an observer at the point $x \ll 0$ at the left side outside the plasma. The reflected field component is given by

$$E_T(x,t) = \frac{a_0^2\sin\alpha}{8}\frac{\lambda}{d_L}\sin[k_l(x+ct)]. \tag{18}$$

From Eq. (18) we can see that the frequency of terahertz emission is only related to the duration of long incident laser pulses, rather than the electron plasma frequency. This explains the simulation results above. Notice there is no terahertz emission for normal incidence or $\alpha = 0$, which is different from surface depletion field and photo-Dember mechanisms in semiconductors [16]. For normal incidence of laser pulses onto plasma, the pure longitudinal current $-env_x$ is canceled completely by the displacement current $\partial E_x/\partial t$. As a result, there is no electromagnetic emission in this case.

For short laser pulses with $k_p^2 \ll k_l^2$, the scalar potential and the electric field corresponding to the reflected emission can be approximated by

$$\varphi(x,t) \simeq \frac{a_0^2\cos\alpha}{4}\{1 - \cos[k_p(x-ct)]\}, \tag{19}$$

$$E_T(x,t) \simeq \frac{a_0^2\sin\alpha}{8}\frac{\lambda}{\lambda_p}\sin[k_p(x+ct)]. \tag{20}$$

From Eq. (20), we can see that for short laser pulses, the radiation frequency is decided by initial plasma density through $k_p \propto \sqrt{n}$, which is consistent with Refs. [11,12].
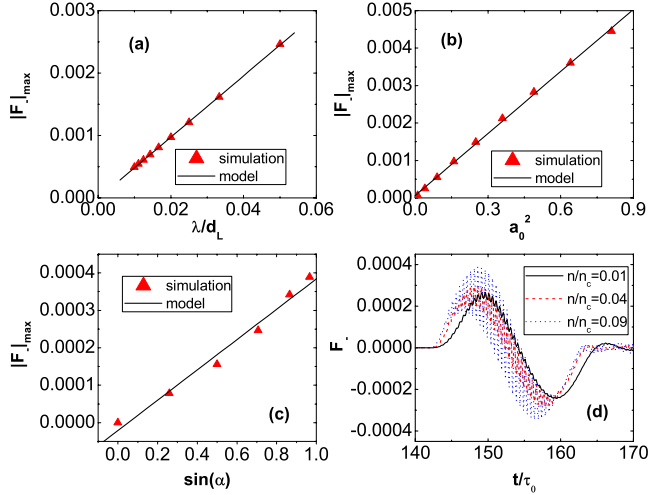
FIG. 3. (Color online) (a) Peak field $|F_-|_{max}$ of the terahertz pulses as a function of the inversion of laser durations. The plasma density is $n/n_c = 0.01$ and the laser has $a_0 = 0.2$ and $\alpha = 45°$. (b) $|F_-|_{max}$ as a function of the laser intensity for $n/n_c = 0.01$, $\tau_L = 20\tau_0$, and $\alpha = 45°$. (c) $|F_-|_{max}$ as a function of $\sin\alpha$ with $\alpha \in [0°, 15°, 30°, 45°, 60°, 75°]$ for $n/n_c = 0.01$, $a_0 = 0.2$, and $\tau_L = 20\tau_0$. (d) Temporal profiles of F_- for $a_0 = 0.2$, $\tau_L = 20\tau_0$, and $\alpha = 45°$ and different plasma densities $n/n_c = 0.01$, 0.04, and 0.09.

C. Comparison between the model and simulations

In the following, we compare the analytical results given by Eqs. (18) and (20) with numerical simulations. Figures 3(a)–3(c) show that the peak field strengths $|F_-|_{max}$ are proportional to the inversion of the laser durations d_L, the laser intensity a_0^2, and $\sin\alpha$, as predicted by Eq. (18). Figure 3(d) illustrates the effect of plasma density. One can easily note that when plasma density increases from $n/n_c = 0.04$ to $n/n_c = 0.09$, the terahertz pulse profile does not change except for the enhancement of 2ω oscillation modulation in the emitted pulses. This indicates that the terahertz-emission strength and frequency have no relation with initial plasma density for long laser pulses. When the emission frequency is lower than the plasma frequency, only the plasma region from the surface to a depth of $d_L \cos\alpha$ participates in the generation of the emission.

When plasma density is not uniform and increases linearly in a length much longer than plasma wavelength, linear mode conversion mechanism takes the main role of terahertz emission. In Fig. 4, we compare our schemes with linear mode conversion for different density profiles. The single-cycle pulse is radiated from a homogeneous plasma with the density $n/n_c = 0.01$ in $x \in [100\lambda, 200\lambda]$. The multicycle pulse is produced by linear mode conversion in an inhomogeneous plasma slab with density linearly increasing from 0 to $0.01n_c$ in $x \in [100\lambda, 200\lambda]$. Note that the peak fields emitted from both schemes are nearly equal. If the initial density is trapezoid with a linearly rising part near the surface, the emission pulse is still single cycle and similarly as with the case of homogeneous plasma. This implies that the density homogeneity of the plasma slab is not necessary. However, it demands that the length of the linearly rising part is shorter than the radiation wavelength. One notes that the emission
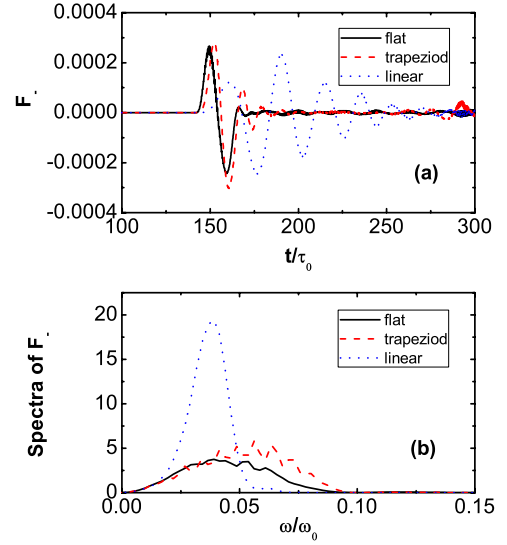

FIG. 4. (Color online) Comparison of (a) temporal profiles and (b) power spectra (arbitrary units) of F_- from different density profiles. The flat plasma profile (solid lines) represents a homogeneous plasma slab with $n/n_c = 0.01$ from $x = 100\lambda$ to $x = 200\lambda$. The trapezoid profile (dashed lines) linearly rises from 0 to $0.01n_c$ for $x \in [100\lambda, 105\lambda]$ and remains uniform for $x = 200\lambda$. The linear profile (dotted lines) rises linearly from 0 to $0.01n_c$ for $x \in [100\lambda, 200\lambda]$. In all three cases, we take $a_0 = 0.2$ and $\alpha = 45°$.

spectrum from the present mechanism is shifted to a higher-frequency regime and becomes broader than that from the linear mode conversion case.

Figure 5(a) illustrates the temporal profiles of the terahertz pulses with short laser duration $\tau_L = 20\tau_0$ in much more underdense plasma such as $n/n_c = 0.0001$, 0.0004, and 0.0009, where we also take $a_0 = 0.2$ and $\alpha = 45°$. We find that as the plasma density increases, the radiation pulse becomes stronger. Figure 5(b) shows that the central frequency of the
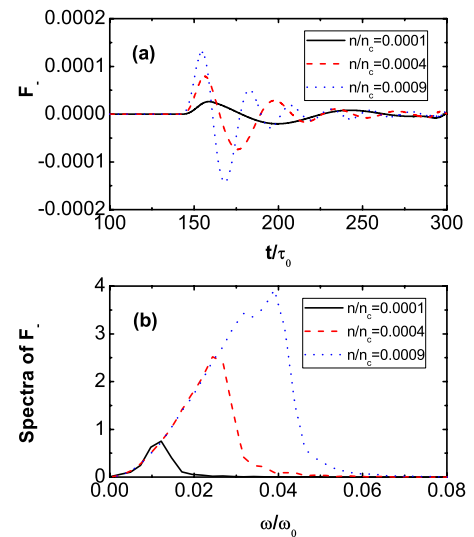

FIG. 5. (Color online) (a) Temporal profiles of the backward emission F_- at the angle of 45° for $a_0 = 0.2$, $\tau_L = 20\tau_0$, and $\alpha = 45°$ and different plasma densities $n/n_c = 0.0001$, 0.0004, and 0.0009. (b) Power spectra (arbitrary units) of F_- in (a).

terahertz spectra is just the plasma frequency, which agrees with Eq. (20).

III. 2D PARTICLE-IN-CELL SIMULATIONS

It should be pointed out that the above 1D model and 1D PIC simulations are valid as long as the laser spot size is large compared with the terahertz wavelength. For a laser beam with a Gaussian profile $\exp(-r^2/W_L^2)$ in transverse space, the 1D model applies for $W_L \gg d_L$. It is easily understood that for $W_L < d_L$, the radiation source size is smaller than the radiated wavelength, so the generated terahertz wave will diffract dramatically. In order to obtain collimated terahertz emission, $W_L \gg d_L$ should be maintained [12].

For 1D case, there is terahertz emission only when the laser is obliquely incident onto the plasma slab. However, in 2D space, because of the finite beam diameter, the ponderomotive force has a transverse component which can drive transverse current, equivalent to the oblique incidence of the laser pulse. In this case, instead of collimated emission, conical terahertz emission with radial polarization is obtained. In the following we present 2D PIC simulation results with normal-incidence pulses to illustrate some multidimensional properties of the terahertz emission. As shown in Fig. 6, the simulation box is $240\lambda \times 240\lambda$, and the plasma is located in the dotted rectangular region with initial density $n/n_c = 0.01$. The laser pulse is s polarized and has parameters $a_0 = 0.2$, $\tau_L = 20\tau_0$, and $W_L = 20\lambda$. It propagates along the x direction at $y = 120\lambda$. Figure 6(a) shows the generated terahertz magnetic field B_z. It is found that there are indeed two single-cycle terahertz pulses in the reflection and transmission directions. For $\lambda = 1$ μm, the amplitude of terahertz field strength exceeds 6 MV/cm. The induced radiation appears to have a symmetric double-lobe shape corresponding to conical emission. There is no terahertz emission along the beam axis. In the three-dimensional space, because of the axial symmetry of the ponderomotive force, the terahertz electric field would be radially polarized and the magnetic field is in the azimuthal direction. Figure 6(b) shows the evolution of the transverse current j_y at the vacuum-plasma interface $x = 120\lambda$ driven by the transverse ponderomotive force. One notes that the current propagates along the plasma surface with a velocity close to c and decays slowly. This current should be relevant to the propagation of terahertz pulse in vacuum around the plasma surface.

IV. CONCLUSION

To conclude, we have presented a theoretical model for the generation of single-cycle high-power terahertz radiation from a tenuous underdense plasma slab. This radiation is generated by the currents at the vacuum-plasma interface due to the ponderomotive force of the incident laser pulse. It shows that the radiation frequency can be controlled by either the inverse of the laser-pulse duration or the plasma frequency, depending upon their relative magnitudes. The radiation frequency takes the smaller one. The theoretical
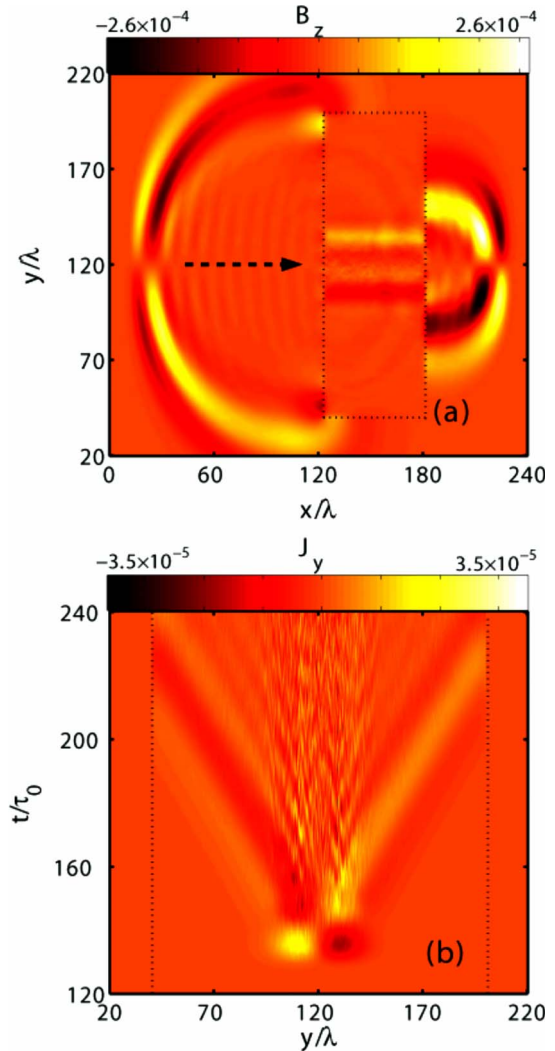

FIG. 6. (Color online) (a) A snapshot of the magnetic component B_z of the terahertz emissions from 2D PIC simulation at $t = 240\tau_0$. The dashed arrow points to the laser incidence direction, and the dotted rectangle marks the plasma surface. (b) Temporal profile of the transverse current J_y along the left boundary $x = 120\lambda$ of the plasma slab.

model is well confirmed by PIC simulation. Our theoretical model is valid for $a_L^2 \ll 1$, or weakly relativistic laser intensities, for example, $\lesssim 10^{17}$ W/cm^2. The latter is usually high enough to produce powerful coherent terahertz sources at a few tens of MW level, suitable for applications in nonlinear and high-field terahertz science.

[1] B. Ferguson and X.-C. Zhang, Nature Mater. **1**, 26 (2002).

[2] H. T. Chen, W. J. Padilla, J. M. O. Zide, A. C. Gossard, A. J. Taylor, and R. D. Averitt, Nature (London) **444**, 597 (2006).

[3] W. P. Leemans, C. G. R. Geddes, J. Faure, Cs. Tóth, J. van Tilborg, C. B. Schroeder, E. Esarey, G. Fubiani, D. Auerbach, B. Marcelis, M. A. Carnahan, R. A. Kaindl, J. Byrd, and M. C. Martin, Phys. Rev. Lett. **91**, 074802 (2003); C. B. Schroeder, E. Esarey, J. van Tilborg, and W. P. Leemans, Phys. Rev. E **69**, 016501 (2004).

[4] G. L. Carr, M. C. Martion, W. R. Mckinney, K. Jordan, G. R. Neil, and G. P. Williams, Nature (London) **420**, 153 (2002); M. Abo-Bakr, J. Feikes, K. Holldack, P. Kuske, W. B. Peatman, U. Schade, G. Wustefeld, and H.-W. Hubers, Phys. Rev. Lett. **90**, 094801 (2003).

[5] J. Yoshii, C. H. Lai, T. Katsouleas, C. Joshi, and W. B. Mori, Phys. Rev. Lett. **79**, 4194 (1997).

[6] H. Hamster, A. Sullivan, S. Gordon, W. White, and R. W. Falcone, Phys. Rev. Lett. **71**, 2725 (1993); H. Hamster, A. Sullivan, S. Gordon, and R. W. Falcone, Phys. Rev. E **49**, 671 (1994).

[7] H. Schillinger and R. Sauerbrey, Appl. Phys. B: Lasers Opt. **68**, 753 (1999).

[8] P. Sprangle, J. R. Penano, B. Hafizi, and C. A. Kapetanakos, Phys. Rev. E **69**, 066415 (2004).

[9] X. Xie, J. M. Dai, and X. C. Zhang, Phys. Rev. Lett. **96**, 075005 (2006).

[10] C. D'Amico, A. Houard, M. Franco, B. Prade, A. Mysyrowicz, A. Couairon, and V. T. Tikhonchuk, Phys. Rev. Lett. **98**, 235002 (2007).

[11] Z.-M. Sheng, K. Mima, J. Zhang, and H. Sanuki, Phys. Rev. Lett. **94**, 095003 (2005); Z.-M. Sheng, K. Mima, and J. Zhang, Phys. Plasmas **12**, 123103 (2005).

[12] H.-C. Wu, Z.-M. Sheng, and J. Zhang, Phys. Rev. E **77**, 046405 (2008).

[13] *Opportunities in THz Science*, Report of a DOE-NSF-NIH Workshop, Arlington, Virginia, 12–14 February, 2004, edited by M. S. Sherwin, C. A. Schmuttenmaer, and P. H. Bucksbaum (http://www.sc.doe.gov/bes/reports/files/THz_rpt.pdf).

[14] Z.-M. Sheng, Y. Sentoku, K. Mima, J. Zhang, W. Yu, and J. Meyer-ter-Vehn, Phys. Rev. Lett. **85**, 5340 (2000).

[15] E. Esarey, P. Sprangle, J. Krall, and A. Ting, IEEE Trans. Plasma Sci. **24**, 252 (1996).

[16] M. B. Johnston, D. M. Whittaker, A. Corchia, A. G. Davies, and E. H. Linfield, Phys. Rev. B **65**, 165301 (2002).

[17] R. Lichters, J. Meyer-ter-Vehn, and A. Pukhov, Phys. Plasmas **3**, 3425 (1996).

[18] P. Sprangle, E. Esarey, and A. Ting, Phys. Rev. A **41**, 4463 (1990).